scientific reports

Check for updates

OPEN

# AI-assisted radiographic analysis in detecting alveolar bone-loss severity and patterns

Chathura Wimalasiri[1,4]✉, Piumal Rathnayake[1,4], Shamod Wijerathne[1,4], Sumudu Rasnayaka[2], Dhanushka Leuke Bandara[2], Roshan G. Ragel[1], Vajira Thambawita[3] & Isuru Nawinne[1]✉

**Periodontitis, a chronic inflammatory disease causing alveolar bone loss which significantly affects oral health and quality of life. Accurate assessment of bone loss severity and pattern is critical for diagnosis and treatment planning. In this study, we propose a novel AI-based deep learning framework to automatically detect and quantify alveolar bone loss and its patterns using intraoral periapical (IOPA) radiographs. Our method combines YOLOv8 for tooth detection with Keypoint R-CNN models to identify anatomical landmarks, enabling precise calculation of bone loss severity. Additionally, YOLOv8x-seg models segment bone levels and tooth masks to determine bone loss patterns (horizontal vs. angular) via geometric analysis. Evaluated on a large, expertly annotated dataset of 1000 radiographs, our approach achieved high accuracy in detecting bone loss severity (intra-class correlation coefficient up to 0.80) and bone loss pattern classification (accuracy 87%). This automated system offers a rapid, objective, and reproducible tool for periodontal assessment, reducing reliance on subjective manual evaluation. By integrating AI into dental radiographic analysis, our framework has the potential to improve early diagnosis and personalized treatment planning for periodontitis, ultimately enhancing patient care and clinical outcomes.**

**Keywords** Artificial intelligence, Deep learning, Computer vision, Alveolar bone loss, Alveolar bone loss patterns, Periapical x-rays, Intraoral periapical radiograph, Periodontitis

The periodontium plays a crucial role in maintaining tooth health by providing structural support, protection, and facilitating the functional integration of teeth within the oral cavity. It consists of four main components: the gingiva, periodontal ligament, cementum, and alveolar bone, each contributing to the overall health and stability of teeth[1]. The health of the periodontium could be affected by several diseases and conditions. The most common disease, periodontitis is a chronic immuno-inflammatory condition which is primarily caused by bacterial infection that leads to progressive destruction of the alveolar bone and periodontal ligament, ultimately resulting in tooth loss if untreated[2].

Severe periodontitis has a global prevalence of about 19% in individuals over 15 years of age and is also the sixth most prevalent disease worldwide[3]. Smoking and uncontrolled diabetes have been identified as risk factors for exacerbation of the disease[4]. Further, it has a major impact on patients' self-esteem since it could eventually lead to tooth loss, which compromises aesthetics and dietary intake[5].

The immuno-inflammatory reactions that occur due to the dysbiosis of the oral biofilm trigger a cascade of reactions that would affect periodontal structures, giving rise to various clinical and radiological presentations[4]. Appropriate evaluation of these clinical and radiographic findings during the patient assessment assists the clinician to arrive at a diagnosis as well as to determine the appropriate treatment plan[2]. Radiological assessments play a pivotal role in periodontal assessment[6]. The most frequently employed techniques include obtaining intra-oral radiographs, including peri-apical and bitewing radiographs[7].

Depending on the probing depths detected, for the sites with deep periodontal pockets, periapical radiographs are usually recommended, while for mild-moderate pocket depths, a bitewing radiograph could be applicable[8]. The identification of alveolar bone loss is critical in periodontal diagnosis, which would reflect as the clinical

[1]Faculty of Engineering, University of Peradeniya, Peradeniya 20400, Sri Lanka. [2]Faculty of Dental Sciences, University of Peradeniya, Peradeniya 20400, Sri Lanka. [3]Simula Metropolitan Center for Digital Engineering, Oslo 0164, Norway. [4]Chathura Wimalasiri, Piumal Rathnayake, and Shamod Wijerathne contributed equally to this work. ✉email: e18402@eng.pdn.ac.lk; isurunawinne@eng.pdn.ac.lk

attachment loss[9]. Therefore, during radiological assessment, the extent of bone loss is assessed aligned with the long axis of the neighboring teeth, by evaluating the vertical distance between the cemento-enamel junction (CEJ) and the alveolar crest[10]. Figure 1a illustrates the key points used to assess alveolar bone loss on an intraoral periapical radiograph (IOPA).

This reduction in bone height also causes changes in the alveolar crestal bone morphology. Understanding the nature of these alterations is essential for effective treatment planning. Radiologically, two main alveolar bone loss patterns could be identified as horizontal or angular (vertical) bone loss[11]. The horizontal pattern shows a uniform reduction in alveolar bone height around the teeth, as seen in Fig. 1c, while the vertical (angular) pattern shows an uneven reduction that creates an angular appearance[12], as shown in Fig. 1d. Clinicians use radiographic analysis to differentiate between these two bone loss patterns, which would assist in treatment planning, especially for periodontal regenerative approaches.

Periodontal disease management is a complex and time-consuming process requiring long-term maintenance following treatment[13]. Early diagnosis and prompt treatment significantly affect the outcome of treatment[14]. Early and accurate detection of periodontitis is critical for effective disease management. Precise determination of the stage and severity of periodontal disease requires comprehensive diagnostic procedures, including detailed assessment of each tooth, owing to the heterogeneous clinical presentation of the condition. Currently, the diagnosis of periodontal disease is based largely on clinical findings and radiographic assessment. Nevertheless, the evaluation of radiographs remains subjective and is affected by factors such as the clinician's level of experience strain or fatigue and the quality of the images obtained [15]. Diagnosis may be difficult owing to a lack of experienced oral or specialist physicians in small clinics/hospitals [16]. Moreover, the identification of periodontal bone loss on radiographs is limited by variable diagnostic accuracy among individual examiners and poor consistency between different observers, as reported across a wide range of studies using diverse reference methods [17]. These limitations highlight the need for more objective, reliable, and efficient diagnostic tools to enhance the accuracy and consistency of periodontal disease detection [15]. At present, artificial intelligence (AI) has emerged as a transformative force, reshaping nearly every aspect of human life[18–20]. AI enables machines to learn from as well as to overcome obstacles by taking inspiration from human cognition, especially the human's capacity for problem-solving[21,22]. Computer vision[23–25], machine learning[26–28], and deep learning (DL) [29–31] are increasingly used in medical image analysis. AI could detect complex information and help to select more suitable treatment options by analyzing individual patient data and medical records[32]. They could also simplify complex processes, solve healthcare problems, and improve patient outcomes around the world[33]. According to DL-based studies, which were carried out using 28 DL-based articles in different fields of dentistry, AI models have shown promising results in dentistry[34,35].

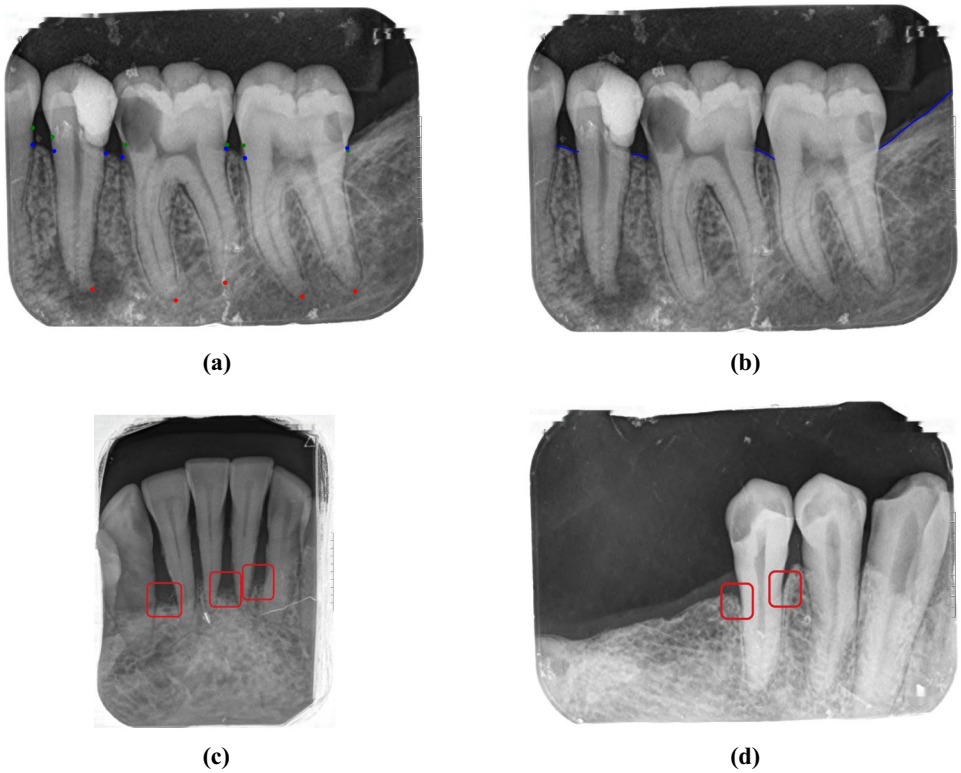


**Fig. 1**. Overview of key features and case classifications used in alveolar bone loss pattern analysis. **a** Key points required for alveolar bone loss analysis; **b** Alveolar bone levels for pattern assessment; **c** Alveolar bone loss cases with horizontal pattern; **d** Alveolar bone loss cases with angular (vertical) pattern.

Recently, the use of AI has been suggested as a supportive tool for clinicians in diagnosing periodontitis and automatically identifying alveolar bone loss[36]. These methods could minimize human error and streamline data analysis as well as task execution[36]. AI systems can also easily record the radiographic images as well as bone loss data of all patients in a database at a dental clinic/hospital with high workload [16]. Table 1 summarizes dataset information, study focus, and key findings of previous studies that had explored various approaches assessing periodontal bone loss. It is worth noting that, although these studies are useful and informative, they also have notable limitations.

Several previous studies[16,37,38] have classified full dental radiographs using binary or multi-class approaches. However, these methods do not provide detailed, tooth-specific, or region-specific information on bone loss, which is essential for accurate periodontal assessment. Several previous studies have used a detection method[39] and a segmentation method[40,45] to identify the bone loss regions. However, these methods also failed to offer a detailed analysis of bone loss at the individual tooth level. Chang et al.[41] used panoramic radiographs to calculate bone loss severity, while Tsoromokos et al.[42], Lee et al.[43], and Chen et al.[44] used peri-apical radiographs to calculate bone loss severity. Tsoromokos et al.[42] assessed radiographs of only mandibular teeth in the analysis. Other types of teeth were excluded to avoid potential data inconsistencies. Kurt-Bayrakdar et al.[45] study elaborates a technique to find the pattern of bone loss in an interdental region defined by the imaginary lines passing through the CEJ points of two adjacent teeth and the alveolar bone crests. If these lines were parallel to each other, bone loss was considered horizontal, whereas if the lines were angular, it was considered vertical. However, the accurate applicability of this method in peri-apical radiographs was limited. Therefore, an improved method is necessary to correctly identify these cases.

Moreover, current studies do not analyze both the severity and patterns of alveolar bone loss using peri-apical radiographs. It is important to identify the alveolar bone loss pattern along with bone loss severity in order to select the correct and effective treatment plan[46]. Understanding the pattern of bone loss aids in planning appropriate interventions, aiming to manage and mitigate the effects of periodontal disease more effectively. To address this gap, we propose a novel AI-based framework for automated assessment of alveolar bone loss severity and patterns using IOPA radiographs. This is very useful for early detection and personalized treatment strategies in periodontal disease management. Our study makes the following contributions:

- We present a novel deep-learning pipeline capable of automating the detection and quantification of both the severity and pattern of alveolar bone loss. To the best of our knowledge, this study is the first to apply DL techniques for the simultaneous prediction of these two critical aspects of alveolar bone loss.
- Our method was evaluated on a large, expertly annotated dataset, and the results demonstrate the effectiveness and validity of our novel approach.
- This study was designed through a collaboration between AI experts and dental professionals to ensure both the technical performance and practical applicability of the findings.

## Materials and methods

### Ethics approval and consent

All methods were carried out in accordance with relevant guidelines and regulations and in compliance with the Declaration of Helsinki. Ethical approval was granted by the Ethics Review Committee, Faculty of Dental Sciences, University of Peradeniya, Sri Lanka (ERC/FDS/UOP/2023/45). As part of the hospital's standard

| Authors Name | Dataset Information | Study Focus and Key Findings |
|---|---|---|
| Bayrakdar et al., 2020[16] | Panoramic Radiographs: Healthy - 1139, Bone Loss - 1137 | Used convolutional neural network model (CNN) to classify healthy and bone loss cases. |
| Sunnetci et al., 2022[37] | Panoramic Radiographs: Healthy - 810, Bone Loss - 622 | Used a hybrid system combining deep learning and machine learning models to classify healthy and bone loss cases. Developed a user-friendly graphical interface. |
| Alotaibi et al., 2022[38] | Periapical Radiographs: Healthy - 814, Bone Loss - 910 (Mild - 511, Moderate - 290, Severe - 109) | Used a CNN network to classify normal and severity of bone loss cases of the anterior region. |
| Ryu et al., 2023[39] | Panoramic Radiographs: 4083 | Grouping teeth into anterior, premolar, and molar regions. Faster R-CNN was used to detect those regions as healthy, edentulous, and periodontitis. |
| Uzun Saylan et al., 2023[40] | Panoramic Radiographs: 685 labeled out of 1543 | YOLO-v5 model detected alveolar bone loss regions of the jaw. |
| Chang et al., 2020[41] | Panoramic Radiographs: 340 | Used a hybrid method combining CNNs with traditional computer aided design (CAD) to classify each tooth into stages of periodontitis. The intraclass correlation (ICC) was 0.91 between the proposed system and the radiologists' diagnoses. |
| Tsoromokos et al., 2022[42] | Periapical Radiographs: 446 | Developed a CNN model to detect and quantify alveolar bone loss (ABL). The ICC was 0.601 across all teeth. The ICC was 0.763 for nonmolar teeth. |
| Lee et al., 2022[43] | Periapical Radiographs: 693 | The U-Net model architectures were used for segmentation tasks. Calculated the severity of radiographic bone loss (RBL) and assigned RBL stages based on the severity of RBL. The Kappa coefficient was 0.81 between the proposed system and the ground truth of RBL stage assignment. |
| Chen et al., 2023[44] | Periapical Radiographs: 8000 | CNN models were used to detect tooth position, detect shape, remaining interproximal bone level, and finally calculate RBL. Research does not fully report descriptive statistics (e.g., ICC, kappa) for comparing predicted and ground truth RBL values. |
| Kurt-Bayrakdar et al., 2024[45] | Panoramic Radiographs: 1121 | A CNN-based system was used to identify total alveolar bone loss region, horizontal bone loss, vertical bone loss, and furcation defect. Area under the ROC curve (AUC) was 0.910, 0.733 for horizontal and vertical bone loss cases, respectively. |

**Table 1**. Overview of studies on the application of deep learning for bone loss detection in radiographs.

registration process, patients provide general (blanket) consent permitting the use of de-identified clinical records, including images, for research and educational purposes. Accordingly, this study used only fully de-identified data and images, and no personal identifiers were retained.

## Dataset overview

The DenPAR dataset[47], consisting of 1000 IOPA radiograph images, was used in this research and is publicly available. The dataset provides multiple forms of ground truth: (i) pixel-level tooth segmentation masks (both radiograph-wise and tooth-wise), (ii) expert-annotated coordinates of the CEJ and apex points, and (iii) alveolar crestal bone-level annotations represented as line coordinates. All annotations were created using the Labelbox tool and were independently verified by dental specialists (MD in Restorative Dentistry and MD in Oral Surgery) to ensure clinical accuracy. Each image is also accompanied by metadata including patient age, sex, arch type, anatomical orientation, and FDI tooth notation. The dataset is pre-split into training (65%), validation (15%), and testing (20%) sets, where the splits were determined through a statistical analysis to ensure balanced distribution across key attributes such as number of teeth, arch type (mandibular or maxillary), root type, and presence of CEJ, apex, and alveolar crestal bone annotations[47]. The official splits are provided in the Zenodo repository, where each subset follows a standardized directory structure (Images, Radiograph-wise Masks, Tooth-wise Masks, Bone Level Annotations, and Key Point Annotations). The annotation files are supplied in widely used formats (PNG masks and COCO-style JSON files), making them directly usable for machine learning experiments. In addition, the repository includes metadata spreadsheets and accompanying GitHub code that allow complete reproducibility of the reported results.

## Calculate alveolar bone loss severity

To identify alveolar bone loss, three specific points needed to be located: i) CEJ, ii) alveolar bone level and tooth intersections, and iii) root apex, as shown in Fig. 1a. First, YOLOv8x was used to detect the rectangular bounding box coordinates of each tooth in the radiographic images. Next, these rectangular bounding box coordinates, along with the radiographic images, were passed to three separate Keypoint R-CNN models. Each model was designed to predict the above-mentioned main types of key points for each tooth. Finally, all the predicted key points were combined to calculate the alveolar bone loss severity. This proposed system is illustrated in Fig. 2a. This diagram illustrates the complete architecture of our system, highlighting key sections such as teeth detection and keypoint detection, combining the separate detected key points, and calculating the alveolar bone loss and its interactions.

### *Implementation of the DL pipeline*

You Only Look Once version 8 (YOLOv8)[48], is a DL model for real-time object detection. YOLOv8 is used in computer vision and DL applications by using a single neural network to predict multiple bounding boxes and class probabilities simultaneously. The YOLOv8x is a variant of YOLOv8 that was used in our proposed system to identify the rectangular bounding box coordinates of each tooth. This approach was necessary because our keypoint detection models were trained on a per-tooth basis. Consequently, three distinct models were used to detect different types of keypoints. In each iteration, a tooth was processed individually through these models to predict the locations of the keypoints.

Three Keypoint R-CNN[49] networks are used to identify these main types of key points separately from radiographs. Keypoint R-CNN, a type of Region-based Convolutional Neural Network, uses the Region of Interest (RoI) Align instead of ROI Pooling to mitigate the misalignment issues that arise due to quantization. This network extends the Faster R-CNN by adding a keypoint head, which is designed to predict the key points associated with detected objects. The outputs of this keypoint head are heatmaps for each keypoint of interest within the object-bounding boxes.

Keypoint R-CNN uses a backbone network to extract features from the input image. In our approach, we used ResNet-50[50] and incorporated another efficient network called a Feature Pyramid Network (FPN)[51] on top of it. Our backbone network extracts convolutional features from the entire input image at multiple scales. This is because ResNet-50 extracts features of the input image at varying levels of abstraction. FPN further enhances these features using feature pyramids that capture information at different spatial resolutions. Hence, ResNet-50 with FPN is the backbone network in our proposed model for keypoint detection.

After the main types of key points are detected separately, the outputs need to be combined to calculate alveolar bone loss. Non-maximum suppression (NMS) [52] was used to achieve this task, using an Intersection over Union (IoU) threshold of 0.6 to filter overlapping key points. NMS is a technique used in object detection tasks, particularly in scenarios where multiple bounding boxes are detected for the same object instance. The primary purpose of NMS is to reduce redundant detections by selecting the most confident bounding boxes that correspond to the same object.

### *Calculating the alveolar bone loss severity using the mathematical approach*

Equation (1) was used for computing alveolar bone loss severity, where a ratio between the pixel distances between points was used. Three points must align along the same line to get the ratio. To achieve this alignment, the min-max line[53] was used, minimizing the maximum error.

$$\text{Alveolar Bone Loss Severity} = \frac{\text{Distance from CEJ to intersection point of tooth boundary and alveolar bone level}}{\text{Distance from CEJ to Apex}} \times 100\% \quad (1)$$

Under this approach, assuming our three points are denoted as $(a_1, b_1)$, $(a_2, b_2)$, and $(a_3, b_3)$, with $(a_1 < a_2 < a_3)$. Then, the gradient of the line is,

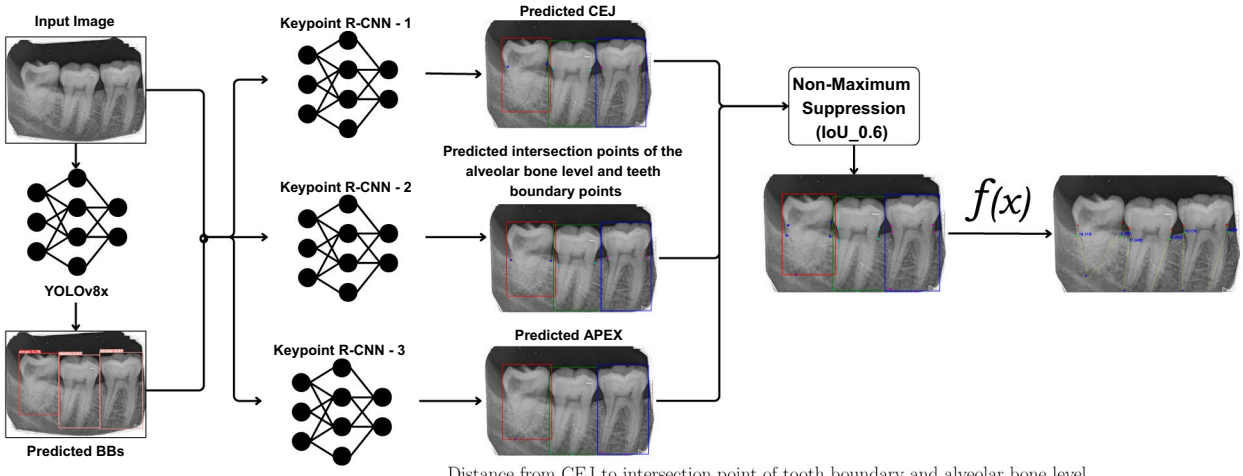


$$f(x)\text{:}Alveolar\ Bone\ Loss\ Severity = \frac{\text{Distance from CEJ to intersection point of tooth boundary and alveolar bone level}}{\text{Distance from CEJ to Apex}} \times 100\%$$

**(a)**

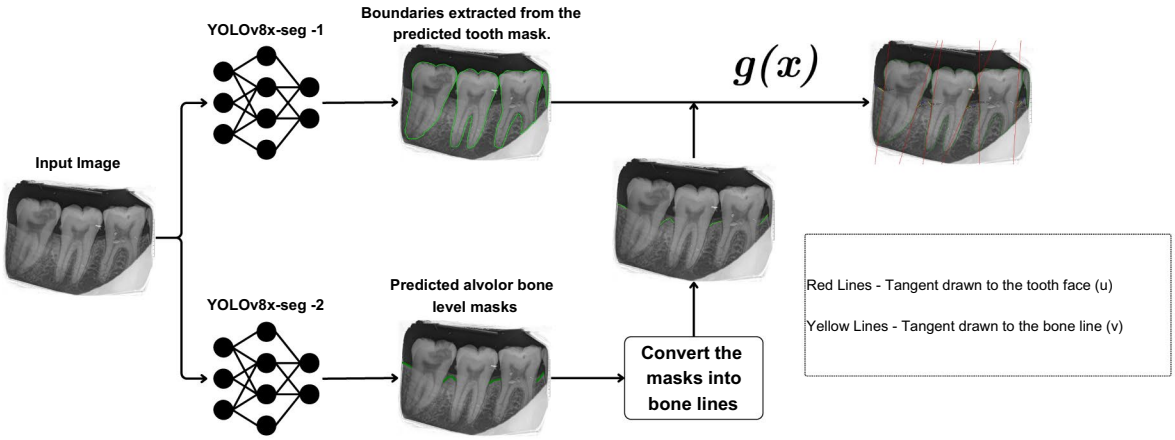


$$g(x)\text{:}Angle\ between\ Tangent\ drawn\ to\ the\ bone\ line\ and\ Tangent\ drawn\ to\ the\ tooth\ face = \cos^{-1}(u \cdot v)$$

**(b)**

**Fig. 2**. Overview of the proposed system: **a** architecture for calculating alveolar bone loss severity; **b** architecture for identifying alveolar bone loss pattern.

$$m = \frac{b_3 - b_1}{a_3 - a_1} \tag{2}$$

And the intercept of the line is,

$$c = \frac{b_1(a_2 + a_3) + b_2(a_3 - a_1) - b_3(a_1 + a_2)}{2(a_3 - a_1)} \tag{3}$$

Figure 3 illustrates that after the min-max line was established, points can be projected onto it perpendicularly. Subsequently, the pixel distance between these points, necessary for determining alveolar bone loss severity, can be measured. This approach allows for the measurement of alveolar bone loss in teeth on both sides.

*Experimental parameter setting*

All experiments were conducted on a Linux based GPU server featuring dual Intel Xeon 4215R processors and two NVIDIA RTX A6000 GPUs with 48 GB of VRAM each. The system was equipped with 128 GB (8× 16 GB) DDR4-2933 memory and a storage configuration consisting of an HP Z Turbo Quad Pro 512 GB SSD and two 4 TB SATA HDDs.

For the tooth detection task, the YOLOv8x used the Adam [54] optimizer and a batch size of 4. The initial learning rates were set to 0.0001 for the model. Additionally, a cosine learning rate scheduler was used. To ensure the best performance of the models, an early stopping method was implemented with a patience size of 25. The

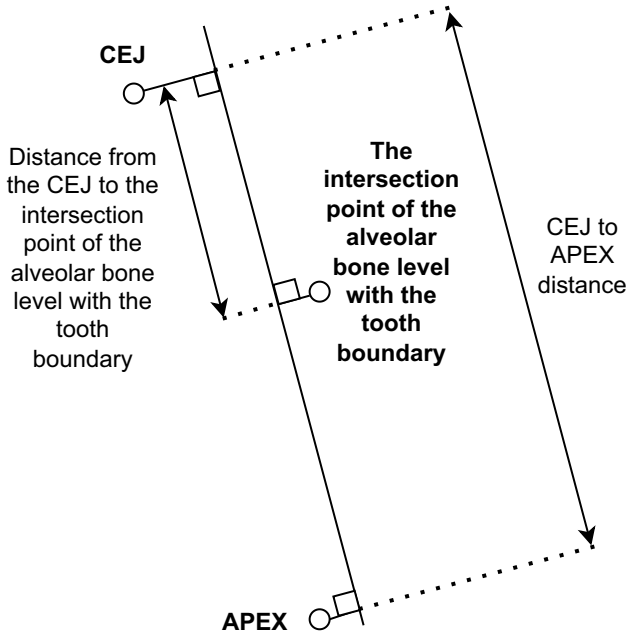


**Fig. 3**. Projection of points onto a minimax line with perpendiculars.

early stopping mechanism further enhanced model performance by preventing overfitting, ensuring that the models were saved at their optimal state.

For the keypoint detection task, Keypoint R-CNN models were set with an initial learning rate of 0.0001 for detecting the CEJ, the intersection point of the tooth boundary and the alveolar bone level, and the root apex. These models used the StepLR learning rate scheduler with a gamma value of 0.6 and a step size of 4. All models were trained using the Adam optimizer with a batch size of 8. To ensure the best performance of the models, an early stopping method was implemented with a patience size of 30. All hyperparameters not explicitly stated follow the default settings of the corresponding frameworks.

## Finding alveolar bone loss pattern

To determine the bone loss pattern in a detected bone loss case, the bone level of the affected region must first be identified. In our approach, YOLOv8x-seg was used to identify the bone levels at affected sites, along with the tooth masks of the relevant teeth. An example of the bone level representation is shown in Fig. 1b. Then, tooth masks were converted into polygons, representing the tooth outlines. Subsequently, by drawing two tangents at the intersection point of the tooth boundary and alveolar bone level, the bone loss angle was calculated. Using the reference values related to this bone loss angle, the pattern was finally determined. An overview of the proposed system is illustrated in Fig. 2b. This diagram shows the complete architecture of the proposed system, highlighting key components such as bone-level line prediction, tooth mask prediction, and the geometrical approach used for bone loss pattern identification.

*Implementation of the DL models*

In a single radiograph, there can be multiple regions affected by alveolar bone loss. To detect the bone loss patterns in these regions, all the relevant bone level lines must be identified. In this case, an instance-segmentation approach was followed. This involved training a YOLOv8x-seg model using the bone-level segmentation masks as inputs.

YOLOv8x-seg is a variant of the YOLOv8, designed specifically for the dual tasks of object detection and instance segmentation. One of the important features of YOLOv8x-seg is its ability to perform instance segmentation. This allows for the accurate identification of object boundaries within images. This is very useful for applications requiring detailed object identification.

Since the dataset only contained alveolar bone levels represented as lines, a data pre-processing method was needed to convert these bone lines into segmentation masks. On the left side of Fig. 4a is the binary mask created using the bone line annotations as they are. By applying the pre-processing method, the thickness of the bone lines was increased to 10 pixels, creating a more visible set of binary masks without losing the basic shape of the bone level line, as shown on the right side of Fig. 4b. All these bone lines are drawn only in the gaps between the teeth.

On the left side of Fig. 4b is a set of bone-level segmentation masks predicted by the DL model. To perform the bone loss pattern-finding calculation, these segmentation masks needed to be converted into lines. A method was used to extract the central path through each mask along its longest extent, resulting in the desired line representation.

(a) (b)

**Fig. 4**. Steps for converting between lines and segmentation masks: **a** Pre-processing lines into masks, and **b** Post-processing masks back into lines.

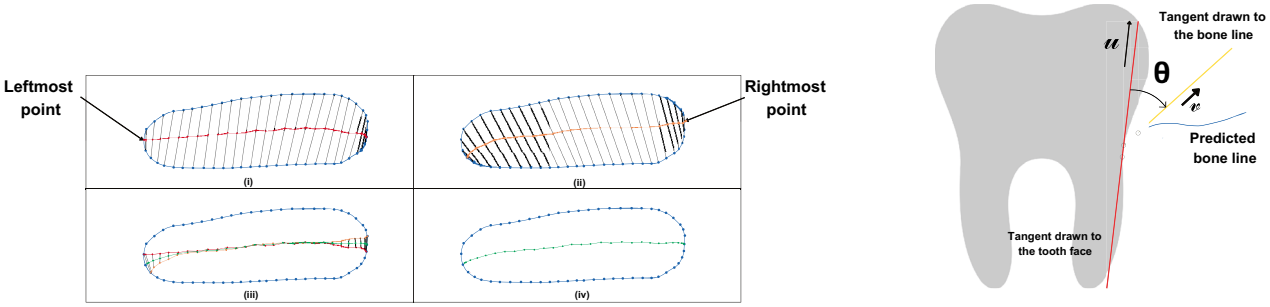


(a) (b)

**Fig. 5**. **a** Method for converting bone level segmentation masks into bone level lines. **b** Geometrical method for calculating the bone loss angle.

The method for this conversion begins by identifying the leftmost point on the mask boundary. Each point before and after this initial point is paired sequentially, continuing in this manner with subsequent outer points on both sides (for example, pairing the second point before with the second point after, the third point before with the third point after, etc.), as indicated by the dotted lines in subfigure (i) of Fig. 5a. The midpoint of each pair is then determined, and these midpoints are connected to form a new line, represented as a red line in subfigure (i) of Fig. 5a.

To ensure a more balanced approach, the same procedure is repeated starting from the rightmost point, resulting in a second line as shown in subfigure (ii) of Fig. 5a. An average line is then created by calculating the mean of the corresponding points on both lines, as illustrated in subfigure (iii) of Fig. 5a, which yields a final line similar to the green line represented in subfigure (iv) of Fig. 5a. This method is applied to all the bone segmentation masks identified in the dental radiographs, thereby transforming them into bone-level lines, as shown on the right side of Fig. 4b.

In addition to identifying the bone level lines, the tooth boundary needed to be identified to determine the bone loss pattern, as it is defined relative to the respective tooth face. To identify the tooth outline, YOLOv8x-seg was also used. The tooth masks obtained through the YOLOv8x-seg were converted into polygons, representing the tooth outlines.

*Determining the bone loss pattern using the mathematical approach*

After identifying the bone level lines and the tooth outlines, a geometrical method was applied to determine the bone loss pattern. This was carried out at the locations where the bone loss was detected via the bone loss severity calculations. As represented in Fig. 5b, first, a tangent line (yellow) was drawn to the predicted bone line (blue) at the intersection point of the predicted tooth boundary and the alveolar bone level.

Next, a tangent line to the tooth face was drawn, as shown in red in Fig. 5b. Similar to the bone line tangent, this line was drawn at the intersection point of the predicted tooth boundary and the alveolar bone level.

After drawing the two tangent lines, the unit vectors along the two lines were calculated. The unit vector along the tooth face tangent was always taken in such a way that it would be in the direction from the tooth crest to the tooth crown. The unit vector along the tangent drawn to the bone line was taken in such a way that it would always direct away from the tooth face.

After finding the two unit vectors, the vector dot product was used to determine the angle between the two vectors, as shown in (4), which was used as an indicator for the bone loss pattern. To determine the decision threshold, this geometrical method was applied to all 720 ground-truth annotations provided by dental experts. The calculated angle values for both angular and horizontal cases were then plotted, as shown in Fig. 6. From this distribution, a clear separation between the two groups was observed, and the intersection point was found at

$54.1372^{\circ}$. This value was therefore selected as the threshold. If $\theta \leq 54.1372^{\circ}$, the case was identified as angular bone loss, while if $\theta > 54.1372^{\circ}$, it was identified as horizontal bone loss. The same geometrical method was then applied to all detected bone loss cases to determine their patterns.

$$\theta = \cos^{-1}(u \cdot v) \tag{4}$$

where $\theta$ is the angle between two vectors, and u and v are unit vectors taken from the two tangents.

*Experimental parameter setting*
All experiments were conducted on the same linux based GPU server setup described in the *Calculate alveolar bone loss severity* section.

To individually identify each tooth and bone line mask, YOLOv8x-Seg used the Adam optimizer with a batch size of 4. The initial learning rate was set to 0.0001, and a cosine learning rate scheduler was applied. Additionally, an early stopping method with a patience of 30 epochs was implemented to ensure optimal performance. All hyperparameters not explicitly stated follow the default settings of the corresponding frameworks.

### Validation of clinical utility of the AI model

In order to assess the clinical unitily of the AI model two sets of experiments were carried out. Twenty five IOPA were selected from the patient database that were not included in the original dataset. Each radiograph was annonymized and the tooth surfaces were marked. The expert (DLB) was requested to assess and record the bone loss percentage and pattern for each tooth surface manually. Same was done using the newly developed AI model. Statistical anaysis was carried out inorder to find the correlation between expert and AI.

## Results

### Tooth detection

First, tooth bounding box detection was performed using three models: i) YOLOv8n, ii) YOLOv8x, and iii) YOLOv9e. These are different variants of YOLOv8 and YOLOv9[55]. All three models were trained under identical parameter settings, including initial learning rate, batch size, optimizer, scheduler, and patience. The quantitative results are reported in Table 2. On the test set, YOLOv8x achieved a precision of 0.892, mAP50 of 0.963, and mAP50:95 of 0.907. YOLOv8n achieved a precision of 0.918, mAP50 of 0.963, and mAP50:95 of 0.894, while YOLOv9e achieved a precision of 0.913, mAP50 of 0.960, and mAP50:95 of 0.904.

To assess whether these differences were statistically significant, we performed paired hypothesis testing on the test set using per-image Average Precision (AP) $_{50:95}$ values, with YOLOv8x as the reference model. The resulting $p$-values were $3.91 \times 10^{-35}$ for YOLOv8n and $4.4 \times 10^{-51}$ for YOLOv9e, indicating statistically significant performance differences relative to YOLOv8x. Figure 7 shows example predictions of YOLOv8x compared with ground truth annotations.

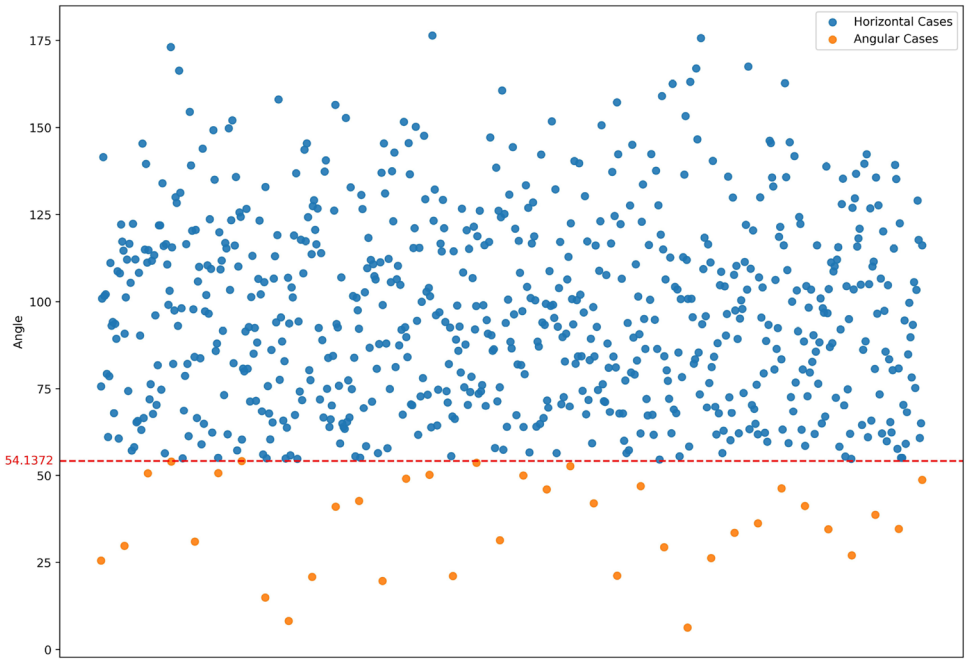


**Fig. 6**. Angle values of ground-truth horizontal and angular cases.

| Model name | Data set type | Precision | mAP50 | mAP50:95 | p-value (vs YOLOv8x) |
|---|---|---|---|---|---|
| YOLOv8x | Train | 0.971 | 0.988 | 0.954 | - |
| | Validation | 0.899 | 0.963 | 0.904 | - |
| | Test | 0.892 | **0.963** | **0.907** | - |
| YOLOv8n | Train | 0.928 | 0.976 | 0.916 | - |
| | Validation | 0.923 | 0.966 | 0.891 | - |
| | Test | **0.918** | **0.963** | 0.894 | $3.91 \times 10^{-35}$ |
| YOLOv9e | Train | 0.985 | 0.991 | 0.966 | - |
| | Validation | 0.911 | 0.967 | 0.908 | - |
| | Test | 0.913 | 0.960 | 0.904 | $4.4 \times 10^{-51}$ |

**Table 2**. Comparison of tooth detection results across different models. Evaluation metrics include precision, mean average precision at the IoU threshold of 0.5 (mAP50) , and Mean Average Precision (mAP) across different IoU thresholds (from 0.5 to 0.95). The *p*-values denote statistically significant differences relative to YOLOv8x on the test dataset.

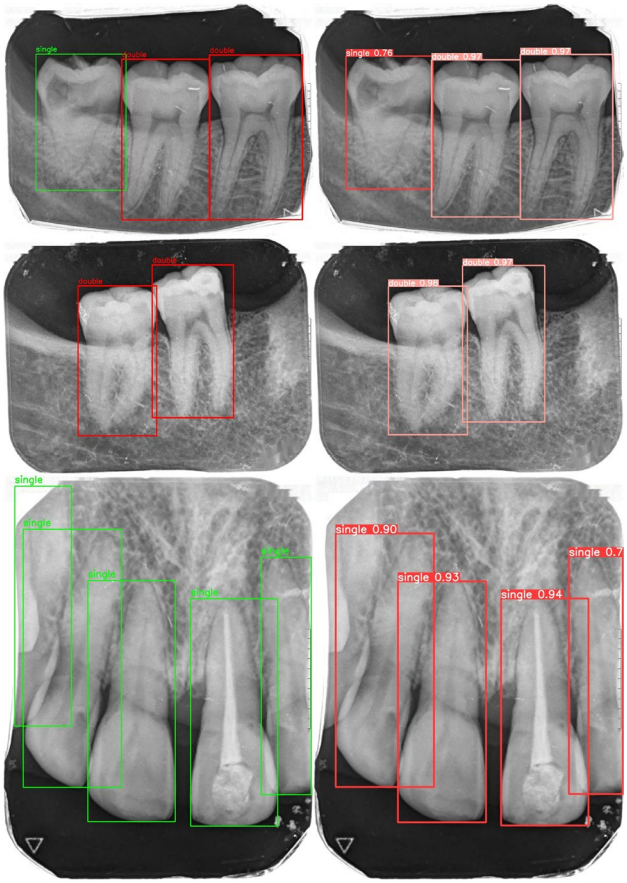


**Fig. 7**. Comparison of ground truth (left) and predicted (right) tooth detection.

## Keypoint detection

Keypoint R-CNN and YOLOv8x-Pose[56] were experimented to detect main types of keypoints. For evaluation, , Object Keypoint Similarity (OKS) was used as the threshold to evaluate the key points. OKS is considered the IoU in keypoints[56]. By considering variables such as scale, unlabeled keypoints, and annotation ambiguity, OKS provides a standardized metric for comparing predicted keypoints against ground truth[57]. Both models were trained under identical settings, except for the learning rate and scheduler (the initial learning rate was 0.00001, and a Cosine learning rate were used for YOLOv8x-Pose).

The results are presented in Table 3. On the test dataset, Keypoint R-CNN achieved AP50:95 scores of 0.954 for CEJ, 0.912 for intersection point of tooth boundary and alveolar bone level, and 0.815 for apex points. YOLOv8x-Pose achieved AP50:95 scores of 0.828, 0.813, and 0.498 for the same keypoints, respectively.

| Keypoint Type | Data set Type | Keypoint R-CNN | | | YOLOv8 Pose | | | |
|---|---|---|---|---|---|---|---|---|
| | | AP50:95 (OKS) | AP50 (OKS) | AP75 (OKS) | AP50:95 (OKS) | AP50 (OKS) | AP75 (OKS) | p-value (vs Keypoint RCNN) |
| CEJ | Train | 0.958 | 0.958 | 0.958 | 0.849 | 0.851 | 0.849 | - |
| | Validation | 0.913 | 0.913 | 0.913 | 0.836 | 0.851 | 0.840 | - |
| | Test | **0.954** | **0.957** | **0.957** | 0.828 | 0.843 | 0.835 | $3.76 \times 10^{-9}$ |
| Intersection point of tooth boundary and alveolar bone level | Train | 0.948 | 0.948 | 0.948 | 0.821 | 0.835 | 0.821 | - |
| | Validation | 0.913 | 0.913 | 0.913 | 0.818 | 0.844 | 0.815 | - |
| | Test | **0.912** | **0.913** | **0.913** | 0.813 | 0.831 | 0.812 | $2.55 \times 10^{-5}$ |
| Apex | Train | 0.862 | 0.867 | 0.861 | 0.554 | 0.583 | 0.548 | - |
| | Validation | 0.847 | 0.855 | 0.848 | 0.470 | 0.505 | 0.466 | - |
| | Test | **0.815** | **0.821** | **0.815** | 0.498 | 0.547 | 0.478 | $4.01 \times 10^{-2}$ |

**Table 3**. Comparison of keypoint detection results across different models. The evaluation metric includes AP across different OKS thresholds (from 0.5 to 0.95), AP at OKS = 0.5 (AP50 (OKS)), and AP at OKS = 0.75 (AP75 (OKS)). The *p*-values denote statistically significant differences relative to Keypoint R-CNN on the test dataset.

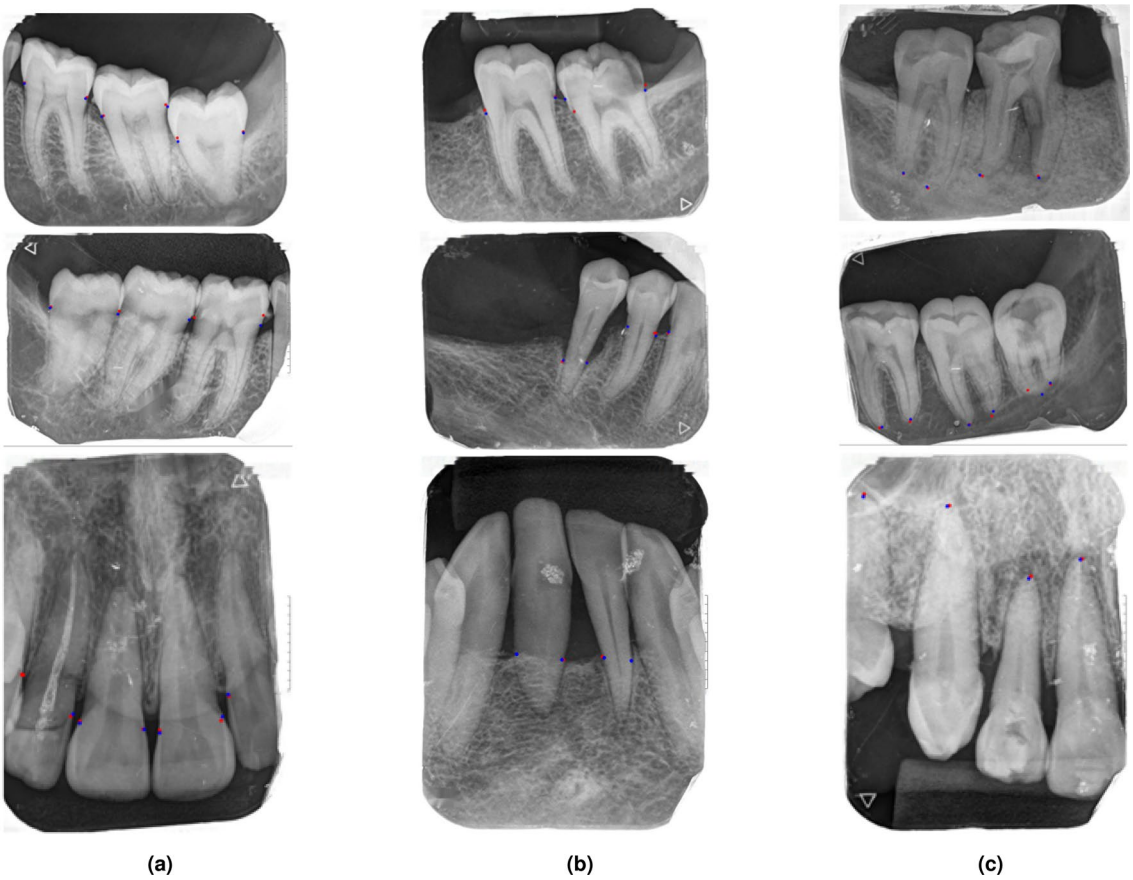


**Fig. 8**. Comparison of ground truth and predicted key points for tooth analysis: **a** cemento-enamel junction (CEJ) points; **b** alveolar bone level and tooth intersection points; **c** apex points. Blue points indicate ground truth, red points indicate predictions.

To assess whether the performance differences between Keypoint R-CNN and YOLOv8 Pose were statistically significant, we computed paired *p*-values on the test set using per-image $AP_{50:95}$ (OKS) scores obtained from YOLOv8 Pose, with Keypoint R-CNN as the reference model. The results showed statistically significant differences across all keypoints, with *p*-values of $3.76 \times 10^{-9}$ for CEJ, $2.55 \times 10^{-5}$ for the intersection point between the tooth boundary and the alveolar bone level, and $4.01 \times 10^{-2}$ for the apex. Figure 8a shows example predictions and ground truth annotations for CEJ, Fig. 8b for the intersection point, and Fig. 8c for the apex.

## Alveolar bone loss severity

The predicted keypoints were used to calculate bone loss severity using the proposed mathematical method. The estimated severity values were compared with ground truth annotations using the Intra-class correlation coefficient (ICC). The ICC values were 0.851, 0.824, and 0.801 for training, validation, and test sets, respectively, indicating consistent agreement. Figure 9 illustrates severity estimations derived from both predicted and ground truth points, including best-fit lines and calculated severity values.

## Tooth and bone line segmentation

YOLOv8x-Seg and Mask R-CNN[49] were trained for tooth and bone line segmentation. The models were trained under different conditions: YOLOv8x-Seg is described in the *Materials and methods* section, while Mask R-CNN was trained with a batch size of 1, a learning rate of 0.00001, and a step scheduler (step size 10, gamma 0.9).

For tooth mask prediction, YOLOv8x-Seg achieved AP50 and AP50:95 scores of 0.978 and 0.900, respectively, on the test dataset, while Mask R-CNN achieved 0.885 and 0.548. For bone line mask prediction, YOLOv8x-Seg achieved AP50 and AP50:95 scores of 0.525 and 0.135, while Mask R-CNN reported 0.005 and 0.001.

To assess whether the performance differences between Mask R-CNN and YOLOv8x-seg were statistically significant, we computed paired $p$-values on the test set using per-image $AP_{50:95}$ values, with YOLOv8x-seg as the reference model. The results showed statistically significant differences for both segmentation tasks, with $p$-values of $3.45 \times 10^{-4}$ for tooth mask segmentation and $1.11 \times 10^{-2}$ for bone line segmentation. These results are summarized in Table 4. Figure 10a shows example predictions and ground truth annotations for tooth boundary segmentation produced by YOLOv8x-seg, while Fig. 10b shows example predictions and ground truth annotations for bone line segmentation.

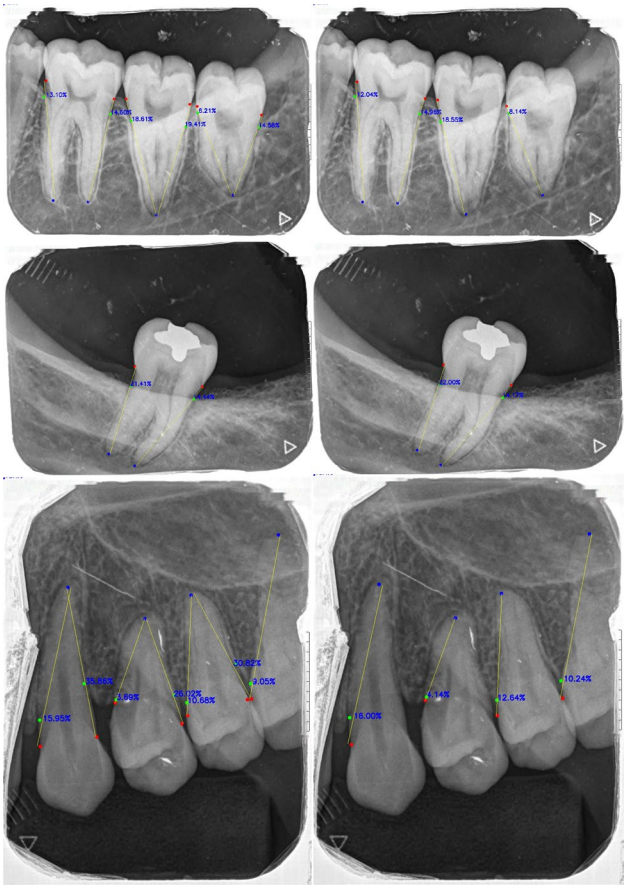

**Fig. 9**. Comparison of ground truth (left) and predicted (right) alveolar bone loss severity. Red points represent the cementoenamel junction (CEJ), green points indicate the intersection between the alveolar crest bone level and the tooth surface, and blue points mark the apex of the tooth. Yellow lines represent the min-max line[53]. Bone loss severity are displayed on the corresponding sides of each tooth. Ground truth severity were calculated using manually annotated points, while predicted severity were derived from the model's predicted points.

| Task | Model name | Data set type | AP50 | AP50:95 | p-value (vs YOLOv8x-seg) |
|---|---|---|---|---|---|
| Tooth Mask | YOLOv8x-seg | Train | 0.995 | 0.962 | - |
| | | Validation | 0.984 | 0.895 | - |
| | | Test | **0.978** | **0.900** | - |
| | Mask RCNN | Train | 0.916 | 0.566 | - |
| | | Validation | 0.903 | 0.532 | - |
| | | Test | 0.885 | 0.548 | $3.45 \times 10^{-4}$ |
| Bone Level Mask | YOLOv8x-seg | Train | 0.697 | 0.202 | - |
| | | Validation | 0.555 | 0.144 | - |
| | | Test | **0.525** | **0.135** | - |
| | Mask RCNN | Train | 0.033 | 0.009 | - |
| | | Validation | 0.011 | 0.004 | - |
| | | Test | 0.005 | 0.001 | $1.11 \times 10^{-2}$ |

**Table 4**. Comparison of tooth and bone level mask prediction results across different models. Evaluation metrics include average precision at the IoU threshold of 0.5 (AP50) and AP across IoU thresholds from 0.5 to 0.95. The *p*-values denote statistically significant differences relative to YOLOv8x-seg on the test dataset.

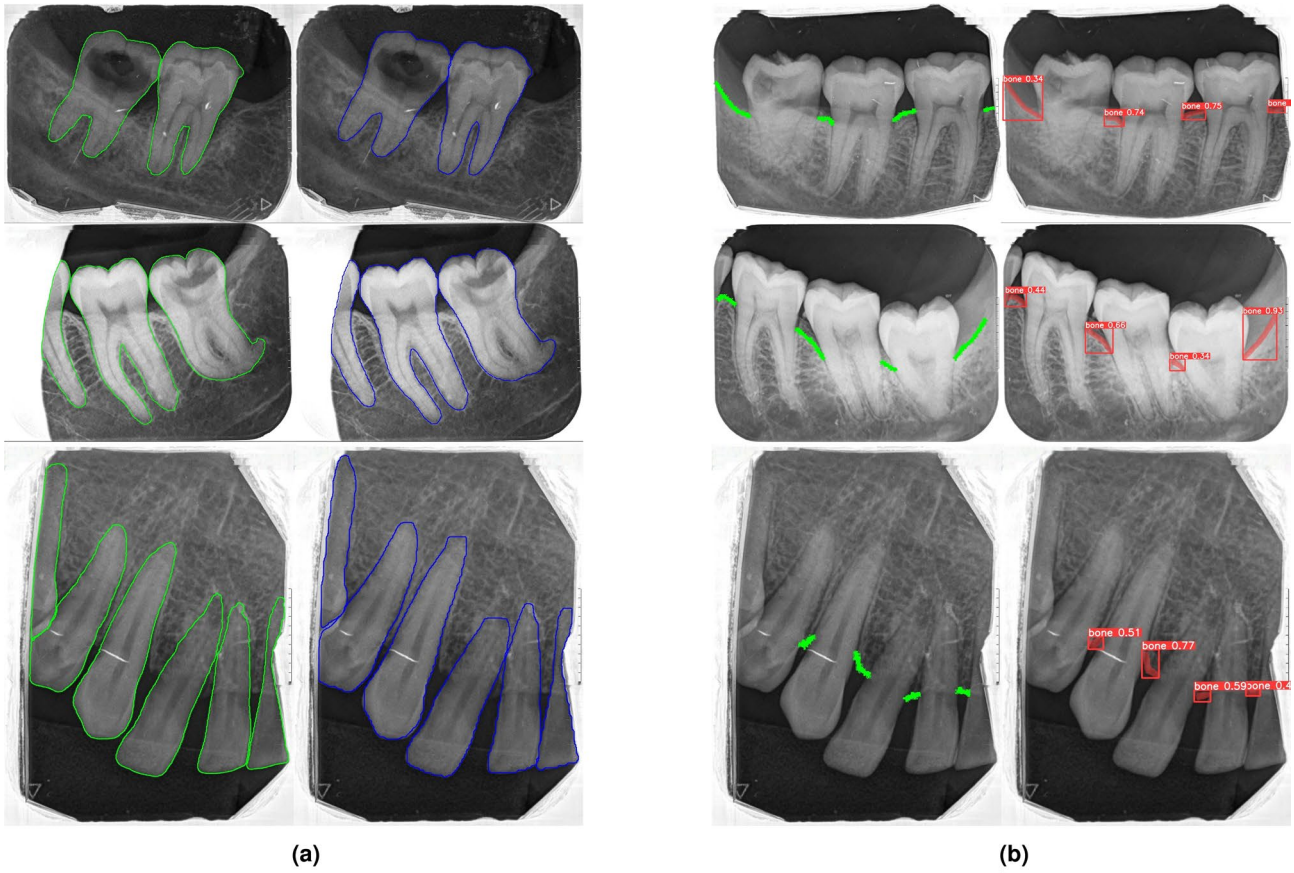


**Fig. 10**. Comparison of ground truth (left) and predicted (right) results: **a** tooth boundaries obtained from the corresponding masks; **b** bone line masks.

## Alveolar bone loss pattern classification

Bone line masks were further converted into line representations, and different thickness values were tested. Table 5 shows the mean squared error (MSE) between predicted and ground truth bone lines for varying thickness values. A thickness of 10 pixels produced consistently lower errors.

Out of 720 expert-annotated cases, 639 were retained for evaluation after excluding incomplete predictions. On this dataset, the proposed method achieved an accuracy of 0.869, precision of 0.985, recall of 0.826, and sensitivity of 0.872. The confusion matrix is presented in Figs. 11, 12 displays the results after applying the

| Thickness value | Train MSE | Validation MSE | Test MSE |
|---|---|---|---|
| 12px | 267.288 | 447.543 | 452.142 |
| 11px | 291.570 | 510.671 | 456.658 |
| 10px | 227.582 | 416.071 | **451.289** |
| 9px | 340.573 | 569.294 | 612.147 |
| 8px | 255.524 | 528.551 | 469.503 |
| 7px | 556.906 | 555.431 | 923.583 |

**Table 5**. Comparison of MSE between ground truth bone line and generated bone line across various pixel levels of masks.

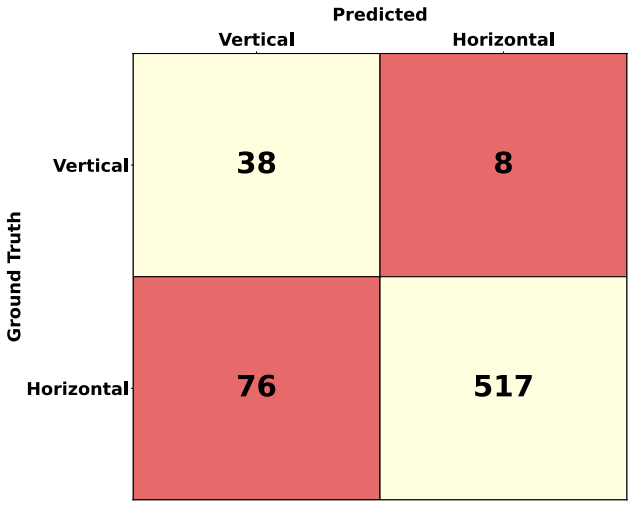


**Fig. 11**. Confusion matrix of ground-truth and predicted horizontal and angular cases, based on 639 total cases provided by dental professionals.

mathematical calculations to the bone level line and tooth boundary results. The left column presents a set of ground truth values for bone loss cases marked by dental professionals, while the right column shows the bone loss cases identified by the proposed methodology. In both columns, red circles indicate angular bone loss, and other markings represent horizontal bone loss.

### Validation of clinical utility

For bone loss severity, we compared the proposed method with expert assessments using Pearson's correlation coefficient ($r$) and the corresponding $p$-value. The results showed a strong correlation ($r = 0.82$) with a statistically significant $p$-value ($2.68 \times 10^{-31}$).

For bone loss pattern (a classification task), we used Cohen's kappa ($\kappa$) and the corresponding $p$-value to compare the proposed method with expert assessments. The method achieved a Cohen's kappa of $\kappa = 0.46$, with a statistically significant $p$-value of $4.24 \times 10^{-5}$.

In addition to predictive accuracy, the time required for interpretation was compared between human experts and the proposed AI system. The expert reported requiring approximately 1 to 4 minutes to interpret a single radiograph, whereas the proposed AI pipeline generated results in approximately 25 seconds per radiograph.

## Discussion

The results highlight the effectiveness of the proposed AI-assisted framework for dental radiographic analysis.

### Tooth detection

YOLOv8x showed the strongest overall detection capability, achieving the highest mAP50 and mAP50:95. While YOLOv8n achieved slightly higher precision, it was less consistent across thresholds. YOLOv9e provided balanced but not leading performance. These results suggest that the YOLOv8x model with higher capacity is better suited for detecting teeth in complex radiographs. Paired statistical comparisons on the test set further provided strong evidence that YOLOv8x outperformed both YOLOv8n and YOLOv9e ($p < 0.001$), indicating that the observed differences are unlikely to be due to random variation in the test data.

### Keypoint detection

Keypoint R-CNN consistently outperformed YOLOv8x-Pose across all three keypoints. This advantage may be attributed to its ROI Align mechanism, which reduces quantization errors and can enable more precise keypoint

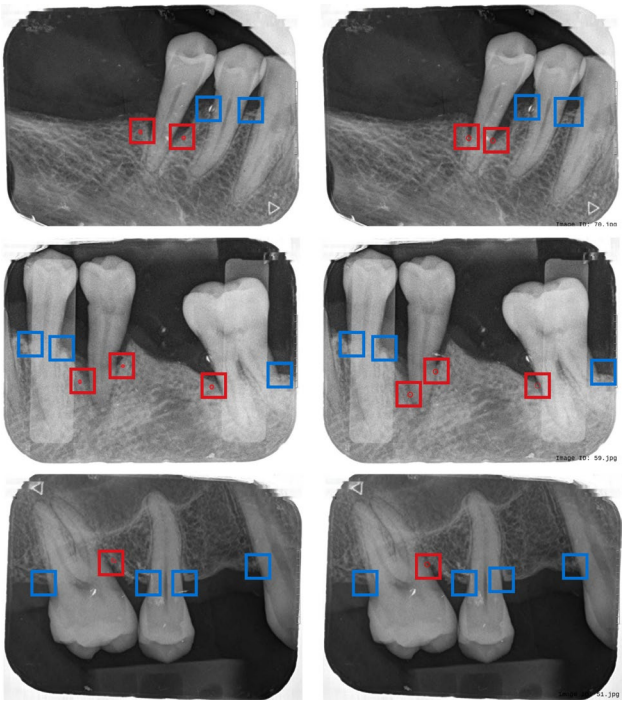

**Fig. 12**. Comparison of bone loss patterns between ground truth (left) and predicted results (right). Red small circles indicate angular bone loss cases predicted by the system. The red rectangle highlights angular bone loss cases, while the blue rectangle highlights horizontal bone loss cases.

localization. Paired statistical testing on the test set provided evidence that the observed performance differences were unlikely to be due to random variation, with $p < 0.05$ for all keypoint types. Accurate detection of the CEJ, the intersection between the tooth boundary and the alveolar bone level, and apex points is essential for reliable bone loss estimation; therefore, the improved keypoint localization achieved by Keypoint R-CNN supports its suitability for clinical radiographic analysis.

### Alveolar bone loss severity

According to Koo and Li (2016)[58], ICC values between 0.75 and 0.90 indicate good reliability. Based on the ICC value from the test set, the proposed severity estimation method produces results consistent with expert evaluations, demonstrating its potential as a decision-support tool for periodontal assessment.

### Tooth and bone line segmentation

YOLOv8x-Seg outperformed Mask R-CNN for both tooth and bone line segmentation. Tooth segmentation was highly accurate, and the pre-processing step of thickening bone lines helped improve prediction quality. Bone lines are thinner, but the model still predicts them well. Paired statistical testing on the test set provided evidence that the observed performance differences were unlikely to be due to random variation ($p < 0.05$), supporting YOLOv8x-seg as a suitable segmentation model for this application.

### Alveolar bone loss pattern classification

The proposed geometrical method achieved an accuracy of $86.9\%$ and very high precision ($98.5\%$) in distinguishing horizontal from angular bone loss. This is clinically significant since bone loss patterns directly influence treatment decisions. The confusion matrix further confirmed balanced performance across both classes.

### Validation of clinical utility

The AI models developed in this study address the challenges of radiographic diagnosis by offering a faster, less labor-intensive, and more precise alternative to conventional diagnostic approaches [15]. The severity results show strong agreement with the expert, with a high correlation ($r = 0.82$) and a highly significant $p$-value ($p < 0.001$), suggesting the proposed method provides severity estimates that are consistent with expert assessment. Simmilarly, an investigation conducted by Lee et al. revealed a diagnostic accuracy of 85%, with no substantial variance observed in the percentage measurements of radiographic bone level between the deep learning algorithm and clinician when utilizing periapical imaging. The study revealed significant sensitivity, specificity, and overall accuracy surpassing 80% across multiple disease stages, and the proposed DL model offered reliable RBL assessments and image-based periodontal diagnosis [43]. A study by Almarghlani compared the ABL measurements between an AI software and practitioners in intra oral radiographs. It was found AI

measurements had a stronger positive correlation with the radiographic measurements (rho 1/4 0.712, p < 0.001) compared with their correlation with the estimates of dental practitioners [59].

For bone loss pattern, the agreement was moderate ($\kappa = 0.46$) and highly significant ($p < 0.001$), indicating that the proposed method shows meaningful concordance with the expert, although pattern classification remains more challenging than severity estimation.

AI systems could be used as a decision-support mechanism for oral physicians. Further, they could capture details overlooked by oral physicians and standardize such decisions. Therefore, applying an AI system for analyzing periodontal diseases from radiographs, could facilitate the early diagnosis, treatment planning, and archiving of information [16]. It offers a promising solution by providing faster, less labor-intensive, and more accurate alternatives to existing methods [15].

### Overall implications

By combining detection, keypoint localization, segmentation, and geometrical analysis, our framework can assess both the severity and pattern of alveolar bone loss in a single system. Unlike previous studies that looked at these aspects separately, this approach provides a more complete and reproducible solution for clinical use in periodontal care.

## Conclusion

In this study, we developed an AI-based method for automatically detecting bone loss patterns and measuring alveolar bone loss severity from IOPA radiographs. According to our results, our deep learning fine-tuned models provide precise and efficient analysis. Such a development can help dentists in the early diagnosis and specific treatment of periodontitis. With the help of deep learning methods and computer vision, our system is capable of detecting both the severity and patterns of bone loss, which are important for differential diagnosis and further treatment planning.

The integration of AI into dental diagnostics is a significant step forward, enhancing the dynamic features of today's healthcare systems. This helps to modernize healthcare practices. Traditional methods of diagnosing alveolar bone loss are mostly time-consuming and depend on the dentist's experience, making them subjective. This could lead to inconsistencies in diagnosis. On the other hand, the AI-based approach presents a standardized, objective, and rapid solution, which increases the reliability in dental assessments.

## Limitations and future work

One limitation of our study is that the AI system was tested mainly on annotated radiographs and hasn't yet been evaluated in real-world clinical settings. In future work, we plan to validate the model in actual dental practices, using a broader range of patient data and real-time diagnostic conditions. We also aim to explore how the system could be integrated into everyday clinical workflows to provide real-time support and monitor alveolar bone-loss progression over time. Tackling these steps will make the tool more practical and reliable for routine dental care.

## Data availability

The dataset used in this study is publicly available on Zenodo at https://doi.org/10.5281/zenodo.16645076.

## Code availability

The deep learning models and algorithms used in this study are available in a public GitHub repository at https://github.com/chathurawimalasiri/analysis-in-detecting-alveolar-bone-loss. The code is compatible with Python 3.10 or later, PyTorch 2.1 or later, Ultralytics YOLOv8, and requires a CUDA-enabled GPU for training and inference. The repository includes training, evaluation, and inference scripts, as well as configuration files specifying model architectures and hyperparameters. It is organized into four main components: (i) tooth detection, (ii) tooth segmentation, (iii) keypoint detection, and (iv) severity and alveolar bone loss pattern calculation. Tooth detection and segmentation are implemented using the YOLOv8 framework, with task-specific parameters provided in the `config.yaml` files. The keypoint detection model is implemented using a Keypoint R-CNN architecture and can be executed via the `main.py` script. The severity and bone loss pattern calculations are implemented as standalone scripts and notebooks. Hyperparameters and training procedures are fully specified in the repository and in the Methods section, enabling full reproducibility of the reported results using the publicly available dataset.

Received: 27 June 2025; Accepted: 28 January 2026
Published online: 09 February 2026

## References

1. Melcher, A. On the repair potential of periodontal tissues. *J. Periodontol.***47**, 256–260 (1976).
2. Milward, M. R. & Roberts, A. Assessing periodontal health and the British society of periodontology implementation of the new classification of periodontal diseases 2017. *Dent. Update***46**, 918–929 (2019).
3. Organization, W.H. *Global oral health status report: towards universal health coverage for oral health by 2030* (World Health Organization, 2022).
4. Matthews, J., Wright, H., Roberts, A., Cooper, P. & Chapple, I. Hyperactivity and reactivity of peripheral blood neutrophils in chronic periodontitis. *Clin. Exp. Immunol.***147**, 255–264 (2007).
5. Kaur, P. et al. Impact of dental disorders and its influence on self esteem levels among adolescents. *J. Clin. Diagn. Res. JCDR***11**, ZC05 (2017).
6. Corbet, E., Ho, D. & Lai, S. Radiographs in periodontal disease diagnosis and management. *Aust. Dent. J.***54**, S27–S43 (2009).

7. Scarfe, W. C., Azevedo, B., Pinheiro, L. R., Priaminiarti, M. & Sales, M. A. The emerging role of maxillofacial radiology in the diagnosis and management of patients with complex periodontitis. *Periodontology***2000**(74), 116–139 (2017).
8. Jacobs, R., Fontenele, R. C., Lahoud, P., Shujaat, S. & Bornstein, M. M. Radiographic diagnosis of periodontal diseases-current evidence versus innovations. *Periodontology***2000**(95), 51–69 (2024).
9. Brägger, U. Radiographic parameters: biological significance and clinical use. *Periodontology***2000**, 39 (2005).
10. Hausmann, E., Allen, K., Carpio, L., Christersson, L. & Clerehugh, V. Computerized methodology for detection of alveolar crestal bone loss from serial intraoral radiographs. *J. Periodontol.***63**, 657–662 (1992).
11. Esmaeli, F. et al. Determination of vertical interproximal bone loss topography: correlation between indirect digital radiographic measurement and clinical measurement. *Iran. J. Radiol.***9**, 83 (2012).
12. Moran, M., Faria, M., Giraldi, G., Bastos, L. & Conci, A. Do radiographic assessments of periodontal bone loss improve with deep learning methods for enhanced image resolution?. *Sensors***21**, 2013 (2021).
13. Tonetti, M. S., Jepsen, S., Jin, L. & Otomo-Corgel, J. Impact of the global burden of periodontal diseases on health, nutrition and wellbeing of mankind: A call for global action. *J. Clin. Periodontol.***44**, 456–462 (2017).
14. Shaddox, L. M. & Walker, C. B. Treating chronic periodontitis: current status, challenges, and future directions. *Clin. Cosmet. Investig. Dent.***2**, 79–91 (2010).
15. Jundaeng, J., Chamchong, R. & Nithikathkul, C. Advanced ai-assisted panoramic radiograph analysis for periodontal prognostication and alveolar bone loss detection. *Front. Dent. Med.***5**, 1509361 (2025).
16. Bayrakdar, İ et al. Success of artificial intelligence system in determining alveolar bone loss from dental panoramic radiography images. *Cumhuriyet Dent. J.* https://doi.org/10.7126/cumudj.777057 (2020).
17. Krois, J. et al. Deep learning for the radiographic detection of periodontal bone loss. *Sci. Rep.***9**, 8495 (2019).
18. Gruetzemacher, R. & Whittlestone, J. The transformative potential of artificial intelligence. *Futures***135**, 102884 (2022).
19. Pachegowda, C. The global impact of ai-artificial intelligence: Recent advances and future directions, a review. arXiv:2401.12223 (2023).
20. Hagerty, A. & Rubinov, I. Global ai ethics: a review of the social impacts and ethical implications of artificial intelligence. arXiv preprint arXiv:1907.07892 (2019).
21. Sen, D., Chakrabarti, R., Chatterjee, S., Grewal, D. & Manrai, K. Artificial intelligence and the radiologist: the future in the armed forces medical services. *BMJ Mil Health***166**, 254–256 (2020).
22. McCarthy, J., Minsky, M. L., Rochester, N. & Shannon, C. E. A proposal for the Dartmouth summer research project on artificial intelligence, august 31, 1955. *AI Magazine***27**, 12–12 (2006).
23. Pomponiu, V., Nejati, H. & Cheung, N.-M. Deepmole: Deep neural networks for skin mole lesion classification. In *2016 IEEE international conference on image processing (ICIP)*, 2623–2627 (IEEE, 2016).
24. Esteva, A. et al. Dermatologist-level classification of skin cancer with deep neural networks. *Nature***542**, 115–118 (2017).
25. Levine, A. B. et al. Rise of the machines: advances in deep learning for cancer diagnosis. *Trends Cancer***5**, 157–169 (2019).
26. Erickson, B. J., Korfiatis, P., Akkus, Z. & Kline, T. L. Machine learning for medical imaging. *Radiographics***37**, 505–515 (2017).
27. Giger, M. L. Machine learning in medical imaging. *J. Am. Coll. Radiol.***15**, 512–520 (2018).
28. Zhang, D., Wu, G. & Zhou, L. *Machine Learning in Medical Imaging* (Springer, 2014).
29. Litjens, G. et al. A survey on deep learning in medical image analysis. *Med. Image Anal.***42**, 60–88 (2017).
30. Shen, D., Wu, G. & Suk, H.-I. Deep learning in medical image analysis. *Ann. Rev. Biomed. Eng.***19**, 221–248 (2017).
31. Suganyadevi, S., Seethalakshmi, V. & Balasamy, K. A review on deep learning in medical image analysis. *Int. J. Multimed. Inf. Retr.***11**, 19–38 (2022).
32. Shiwlani, A., Khan, M., Sherani, A. M. K., Qayyum, M. U. & Hussain, H. K. Revolutionizing healthcare: The impact of artificial intelligence on patient care, diagnosis, and treatment. *JURIHUM J. Inov. Hum.***1**, 779–790 (2024).
33. Ahmed, N. et al. Artificial intelligence techniques: analysis, application, and outcome in dentistry—a systematic review. *BioMed Res. Int.***2021**, 9751564 (2021).
34. Farook, T. H., Jamayet, N. B., Abdullah, J. Y. & Alam, M. K. Machine learning and intelligent diagnostics in dental and orofacial pain management: A systematic review. *Pain Res. Manag.***2021**, 6659133 (2021).
35. Corbella, S., Srinivas, S. & Cabitza, F. Applications of deep learning in dentistry. *Oral Surg. Oral Med. Oral Pathol. Oral Radiol.***132**, 225–238 (2021).
36. Revilla-León, M. et al. Artificial intelligence models for diagnosing gingivitis and periodontal disease: A systematic review. *J. Prosthet. Dent.***130**, 816–824 (2023).
37. Sunnetci, K. M., Ulukaya, S. & Alkan, A. Periodontal bone loss detection based on hybrid deep learning and machine learning models with a user-friendly application. *Biomed. Signal Process. Control***77**, 103844 (2022).
38. Alotaibi, G. et al. Artificial intelligence (ai) diagnostic tools: Utilizing a convolutional neural network (cnn) to assess periodontal bone level radiographically—a retrospective study. *BMC Oral Health***22**, 399 (2022).
39. Ryu, J. et al. Automated detection of periodontal bone loss using deep learning and panoramic radiographs: a convolutional neural network approach. *Appl. Sci.***13**, 5261 (2023).
40. Uzun Saylan, B. C. et al. Assessing the effectiveness of artificial intelligence models for detecting alveolar bone loss in periodontal disease: a panoramic radiograph study. *Diagnostics***13**, 1800 (2023).
41. Chang, H.-J. et al. Deep learning hybrid method to automatically diagnose periodontal bone loss and stage periodontitis. *Sci. Rep.***10**, 7531 (2020).
42. Tsoromokos, N., Parinussa, S., Claessen, F., Moin, D. A. & Loos, B. G. Estimation of alveolar bone loss in periodontitis using machine learning. *Int. Dent. J.***72**, 621–627 (2022).
43. Lee, C.-T. et al. Use of the deep learning approach to measure alveolar bone level. *J. Clin. Periodontol.***49**, 260–269 (2022).
44. Chen, C.-C. et al. Automatic recognition of teeth and periodontal bone loss measurement in digital radiographs using deep-learning artificial intelligence. *J. Dent. Sci.***18**, 1301–1309 (2023).
45. Kurt-Bayrakdar, S. et al. Detection of periodontal bone loss patterns and furcation defects from panoramic radiographs using deep learning algorithm: a retrospective study. *BMC Oral Health***24**, 155 (2024).
46. Jayakumar, A., Rohini, S., Naveen, A., Haritha, A. & Reddy, K. Horizontal alveolar bone loss: A periodontal orphan. *J. Indian Soc. Periodontol.***14**, 181–185 (2010).
47. Rasnayaka, S. et al. Denpar: Annotated intra-oral periapical radiographs dataset for machine learning. *Sci. Data***12**, 1615 (2025).
48. Reis, D., Kupec, J., Hong, J. & Daoudi, A. Real-time flying object detection with yolov8. arXiv preprint arXiv:2305.09972 (2023).
49. He, K., Gkioxari, G., Dollár, P. & Girshick, R. Mask r-cnn. In *Proceedings of the IEEE international conference on computer vision*, 2961–2969 (2017).
50. He, K., Zhang, X., Ren, S. & Sun, J. Deep residual learning for image recognition. In *Proceedings of the IEEE conference on computer vision and pattern recognition*, 770–778 (2016).
51. Lin, T.-Y. *et al.* Feature pyramid networks for object detection. In *Proceedings of the IEEE conference on computer vision and pattern recognition*, 2117–2125 (2017).
52. Hosang, J., Benenson, R. & Schiele, B. Learning non-maximum suppression. In *Proceedings of the IEEE conference on computer vision and pattern recognition*, 4507–4515 (2017).
53. Cook, J.D. Min-max line for three points. Applied Mathematics Consulting. Retrieved July 7 (2023).
54. Kingma, D. P. & Ba, J. Adam: A method for stochastic optimization. arXiv preprint arXiv:1412.6980 (2014).

55. Wang, C.-Y., Yeh, I.-H. & Liao, H.-Y. M. Yolov9: Learning what you want to learn using programmable gradient information. arXiv:2402.13616 (2024).
56. Maji, D., Nagori, S., Mathew, M. & Poddar, D. Yolo-pose: Enhancing yolo for multi person pose estimation using object keypoint similarity loss. In *Proceedings of the IEEE/CVF Conference on Computer Vision and Pattern Recognition*, 2637–2646 (2022).
57. Object Keypoint Similarity in Keypoint Detection — learnopencv.com. (Accessed 04 September 2024). https://learnopencv.com/object-keypoint-similarity/.
58. Koo, T. K. & Li, M. Y. A guideline of selecting and reporting intraclass correlation coefficients for reliability research. *J. Chiropract. Med.***15**, 155–163 (2016).
59. Almarghlani, A. et al. Dental practitioners versus artificial intelligence software in assessing alveolar bone loss using intraoral radiographs. *J. Taibah Univ. Med. Sci.***20**, 272–279 (2025).

## Acknowledgments
The author acknowledges the support received from the LK Domain Registry in publishing this paper.

## Author contributions
C.W., P.R., and S.W. conducted the experiments and literature review, S.R. and I.N. conceptualized the study, I.N., V.T., and R.G.R. provided engineering expertise and resources, S.R. and D.L. provided dental expertise, I.N., S.R., V.T., D.L., and R.G.R provided supervision and reviewed methodologies. All authors contributed to writing and reviewed the manuscript.

## Funding
This study was not funded.

## Declarations

## Competing interests
The authors declare no competing interests.

## Additional information
**Correspondence** and requests for materials should be addressed to C.W. or I.N.

**Reprints and permissions information** is available at www.nature.com/reprints.

**Publisher's note** Springer Nature remains neutral with regard to jurisdictional claims in published maps and institutional affiliations.